

Provable Robustness in Multimodal Large Language Models via Feature Space Smoothing

Song Xia

Nanyang Technological University

Meiwen Ding

Nanyang Technological University

Chenqi Kong

Nanyang Technological University

Wenhan Yang

Peng Cheng Laboratory

Xudong Jiang

Nanyang Technological University

Abstract

Multimodal large language models (MLLMs) exhibit strong capabilities across diverse applications, yet remain vulnerable to adversarial perturbations that distort their feature representations and induce erroneous predictions. To address this vulnerability, we propose the Feature-space Smoothing (FS) and theoretically prove that FS offers certified robustness on the feature representations of MLLMs. Specifically, FS transforms any feature encoder into a smoothed variant that is guaranteed to maintain a certified lower bound on the feature cosine similarity between clean and adversarial representations under ℓ_2 -bounded attacks. Moreover, we indicate that the value of this Feature Cosine Similarity Bound (FCSB) derived from FS can be improved by enlarging the defined Gaussian robustness score on the vanilla encoder. Building upon this, we introduce the Purifier and Smoothness Mapper (PSM), a plug-and-play module that improves the Gaussian robustness score of MLLMs and thus enhances their certified robustness under FS, without requiring any retraining on MLLMs. We demonstrate that the FS with PSM not only provides a strong theoretical robustness guarantee but also exhibits superior empirical performance compared to adversarial training. Extensive experiments across diverse MLLMs and downstream tasks indicate the effectiveness of the FS-PSM, reducing the Attack Success Rate (ASR) of various white-box attacks from nearly 90% to about 1%.

1. Introduction

The emergence of the Multimodal Large Language Models (MLLMs), such as GPT-5, Gemini 2.5, and Claude 3.7 Sonnet, has fundamentally reshaped existing working paradigms and significantly advanced societal productiv-

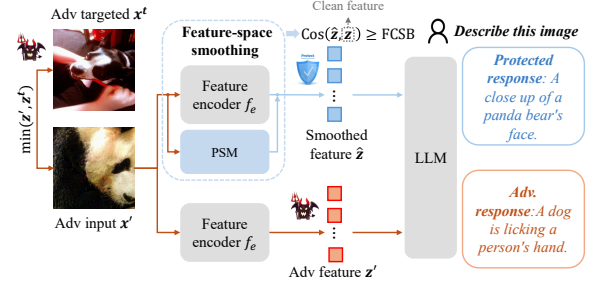


Figure 1. Illustration of the FS-PSM, which guarantees that the cosine similarity of the adversarial and clean features extracted by MLLM’s encoder is larger than FCSB for robust predictions.

ity. Despite their remarkable capabilities across a broad spectrum of real-world tasks, these models still encounter critical safety challenges, such as adversarial vulnerabilities [5, 14, 23, 51]. Adversaries can manipulate predictions of the MLLMs to a malicious state by injecting subtle and imperceptible perturbations to the clean inputs, exploiting the models’ insufficient local smoothness and uncontrolled Lipschitz continuity [4, 10, 12, 47].

Countermeasures towards those threats can be roughly classified into empirical defense and certified defense. Typical empirical approaches include adversarial training [2, 27–29, 35, 37, 41, 45] and input purification [2, 27–29, 35, 37, 41, 45]. Despite their demonstrated empirical effectiveness, the multimodal nature of MLLMs also poses a great challenge for existing adversarial defense methods. Since these models accept heterogeneous inputs across diverse domains, ensure a robust encoder via adversarial training that can generalize to various scenarios is challenging and computationally expensive. Moreover, these approaches lack formal robustness guarantees and remain susceptible to stronger or adaptive adversaries [3, 38, 44]. In contrast,

certified approaches aim to guarantee that the model returns a constant prediction result within a certain range, usually a ℓ_2 or ℓ_∞ -norm constrained area [4, 11, 15, 34, 36, 43, 47]. However, most previous certified defense approaches [4, 11, 36, 42, 47] predominantly assume the prediction of one-dimensional outputs (e.g., class label), thereby limiting their applicability to more general tasks on MLLMs.

To address the aforementioned challenges, we propose the Feature-space Smoothing (FS), a provable defense method that offers certified robustness for the feature representations of MLLMs. FS smooths the vanilla feature encoder of the MLLM, and the resulted smoothed encoder is guaranteed to maintain a provable lower bound on the cosine similarity between clean and adversarial representations under ℓ_2 -norm bounded attacks.

Moreover, we demonstrate that the Feature Cosine Similarity Bound (FCSB) of the smoothed feature encoder is intrinsically determined by a Gaussian robustness score, which is defined to measure the prediction consistency of the vanilla feature extractor under Gaussian noise. Nonetheless, without Gaussian noise-augmented training, the Gaussian robustness of these MLLMs remains limited, leading to a correspondingly suboptimal FCSB. To address this and avoid the heavy computational cost of fine-tuning MLLMs, we propose a plug-and-play Purifier and Smoothness Mapper (PSM) that effectively enhance the Gaussian robustness score for the vanilla feature encoder in a training-free way. Specifically, the purifier operates prior to feature extraction and is trained to denoise Gaussian perturbations and maximize the Gaussian robustness score. Meanwhile, the smoothness mapper performs post-extraction refinement and is trained to preserve the feature distribution while further enhancing this score without fine-tuning the encoder. These two components of PSM work synergistically to enhance the certified robustness of MLLMs under FS.

To implement our PSM, we employ a pre-trained guided diffusion model as the Gaussian noise purifier and design a noise-aware residual network as the smoothness mapper. The PSM is optimized using the proposed utility-robustness loss and trained on data from diverse visual domains to enhance the Gaussian robustness while preserving the feature utility for the encoder. To comprehensively assess the performance, we evaluate our method against state-of-the-art (SOTA) adversarial attacks tailored for MLLMs under the white-box setting and compare it with strong adversarial training defense. Experimental results demonstrate that our FS with PSM enhanced provides strong protection for various MLLMs under diverse downstream tasks. Overall, the main contributions of this work are:

- We propose the Feature-space Smoothing (FS) to turn any feature encoder of MLLMs into a smoothed version, and theoretically prove that the smoothed encoder maintains a certified lower bound on the feature cosine similarity

between clean and adversarial representations.

- We propose a plug-and-play Purifier and Smoothness Mapper (PSM) that effectively enhances the value of the FCSB of the smoothed encoder in a training-free manner.
- We conduct extensive experiments demonstrating that integrating our proposed FS-PSM greatly enhances the adversarial performance of various MLLMs and dramatically reduces the ASR under various white-box attacks.

2. Related Work

Adversarial attacks on MLLMs. While MLLMs continue to achieve remarkable performance across diverse applications, extensive works [5, 14, 23, 31, 39, 48–51] have exposed their adversarial vulnerabilities, raising serious safety concerns. Early work, such as AttackVLM [51], explores transferable attacks by disrupting the feature representations of CLIP [33] and BLIP [19], showing strong adversarial transferability among open-source models but limited effectiveness against closed-source commercial systems. More recent approaches, such as M-Attack [23] and FOA-Attack [14], further advance this direction by leveraging multi-extractor ensembles and feature-space alignment, achieving over 90% targeted attack success rates on image-captioning tasks against powerful closed-sourced commercial MLLMs (e.g., ChatGPT-4o). This highlights an urgent need for trustworthy defenses that provide effective and provable protection for MLLMs.

Adversarial defense on MLLMs. Adversarial defense methods can be broadly classified into empirical and provable approaches. Empirical defenses for MLLMs mainly include adversarial training [2, 27–29, 35, 37, 41, 45], which enhances robustness by augmenting training data with adversarial examples, and input purification [17, 22, 30], which employs generative mechanisms such as diffusion models or autoencoders to recover clean inputs prior to inference. Recent studies [28, 29, 37] have revealed that utilization of adversarially trained CLIP-feature encoders can enhance adversarial robustness for MLLMs. However, these methods lack formal robustness guarantees and remain vulnerable to adaptive and unseen threats [3, 38, 44]. Moreover, adversarial training demands costly retraining and often leads to degradation in clean performance.

Alternatively, certified defenses aim to provide mathematically provable robustness guarantees. The use of Gaussian smoothing for certified robustness was initially introduced for classification models [4, 16, 18], yet its theoretical formulation is restricted to one-dimensional outputs, limiting its applicability to tasks such as auto-regression or multimodal generation. To overcome these limitations and ensure trustworthy protection for MLLMs, we propose the Feature-space Smoothing (FS), a defense mechanism that establishes provable adversarial robustness for MLLMs.

3. Feature Space Smoothing

3.1. Preliminary

Let \mathcal{F} denote a general deep learning model consisting of a feature extractor $f_e : \mathbf{x} \rightarrow \mathbf{z}$ that maps the input \mathbf{x} to a feature representation \mathbf{z} , and a predictor $f_d : \mathbf{z} \rightarrow \mathbf{y}$ that produces the final output \mathbf{y} . Let \mathcal{L} denote the general loss function (e.g., cross-entropy) that measures the discrepancy between the model's output and the ground truth.

Adversarial attacks: Let $\mathcal{B}_\epsilon(\mathbf{x}) = \left\{ \mathbf{x}' : \|\mathbf{x}' - \mathbf{x}\|_p \leq \epsilon \right\}$ be an ℓ_p -norm ball centered at the input \mathbf{x} , where ϵ is a pre-defined perturbation bound. For each input \mathbf{x} , the adversarial attacks aim to find an adversarial input $\mathbf{x}' = \mathbf{x} + \boldsymbol{\delta}$ that misleads the model by solving:

$$\max_{\mathbf{x} + \boldsymbol{\delta} \in \mathcal{B}_\epsilon(\mathbf{x})} \mathcal{L}(\mathcal{F}(\mathbf{x}), \mathcal{F}(\mathbf{x} + \boldsymbol{\delta})). \quad (1)$$

Adversarial effects on feature representations: While adversarial attacks primarily aim to alter the model's predictions, numerous studies [8, 13, 14, 20, 21, 23, 32, 40, 46] have shown that successful attacks typically induce substantial distortions in the model's feature representations. Let \mathbf{x}' denote the adversarial example with adversarial feature \mathbf{z}' . Let \mathbf{z}^t be the adversarial targeted feature with malicious semantic meaning. The attack generally leads to $\max \mathcal{L}(\mathbf{z}', \mathbf{z})$ for untargeted attacks and $\min \mathcal{L}(\mathbf{z}', \mathbf{z}^t)$ for targeted attacks. Thus, ensuring a robust feature encoder that $\min \mathcal{L}(\mathbf{z}', \mathbf{z})$ is crucial for the trustworthy prediction.

Randomized smoothing: Consider a k classes classification problem with the input $\mathbf{x} \in \mathbb{R}^d$ and the label $\mathbf{y} \in \mathcal{Y} = \{c_1, \dots, c_k\}$. Randomized Smoothing (RS) first corrupts each input \mathbf{x} by adding the Gaussian noise $\boldsymbol{\varepsilon} \sim \mathcal{N}(0, \sigma^2 \mathbf{I})$. Then it turns an arbitrary base classifier \mathcal{F} into a smoothed version $\hat{\mathcal{F}}$ that possesses ℓ_2 certified robustness guarantees. The smoothed classifier $\hat{\mathcal{F}}$ returns whichever the class the base classifier \mathcal{F} is most likely to return among the distribution $\mathbf{x} + \boldsymbol{\varepsilon} \sim \mathcal{N}(\mathbf{x}, \sigma^2 \mathbf{I})$, which is:

$$\hat{\mathcal{F}}(\mathbf{x}) = \arg \max_{c \in \mathcal{Y}} \mathbb{P}(\mathcal{F}(\mathbf{x} + \boldsymbol{\varepsilon}) = c). \quad (2)$$

RS then guarantees a certified radius \mathcal{R} for this smoothed classifier $\hat{\mathcal{F}}$. For any perturbation $\boldsymbol{\delta}$ satisfying $\|\boldsymbol{\delta}\|_2 \leq \mathcal{R}$, the smoothed classifier is guaranteed to return a robust prediction that makes $\hat{\mathcal{F}}(\mathbf{x} + \boldsymbol{\delta}) = \mathcal{F}(\mathbf{x})$.

Limitations for RS. While previous RS provides effective certified protection for classification models, it suffers from two limitations. First, the theoretical framework of RS inherently restricts its certification to classification tasks (e.g. possibility of input \mathbf{x} belongs to a certain class c). Second, estimating $\mathbb{P}(\mathcal{F}(\mathbf{x} + \boldsymbol{\varepsilon}) = c)$ in Equation 2, incurs substantial computational overhead, since each estimation requires multiple forward passes through the entire model.

3.2. Certified Bound via Feature Space Smoothing

Considering the limitations inherent in the RS, we introduce the Feature-space Smoothing (FS). By turning any feature encoder f_e into a smoothed version \hat{f}_e , FS theoretically

guarantees that \hat{f}_e maintains a certified lower bound on the cosine similarity between clean and adversarial representations under ℓ_2 -norm constrained perturbations.

Smoothed feature encoder. For any feature encoder $f_e : \mathbf{x} \rightarrow \mathbf{z}$, where \mathbf{z} is the representation normalized into the ℓ_2 unit sphere, FS defines the smoothed encoder $\hat{f}_e(\mathbf{x})$ as:

$$\begin{aligned} \hat{f}_e(\mathbf{x}) &= \mathbb{E}_{\boldsymbol{\varepsilon} \sim \mathcal{N}(0, I)} [f_e(\mathbf{x} + \boldsymbol{\varepsilon})] \\ &= \frac{1}{(2\pi)^{d/2}} \int_{\mathbb{R}^d} f_e(\mathbf{x} + \boldsymbol{\varepsilon}) \exp(-\frac{1}{2}\|\boldsymbol{\varepsilon}\|^2) d\boldsymbol{\varepsilon}, \end{aligned} \quad (3)$$

where I denotes the $d \times d$ identity and $\|\cdot\|$ is the Euclidean norm. $\boldsymbol{\varepsilon} \sim \mathcal{N}(0, I)$ denotes Gaussian noise with zero mean and standard deviation one. The smoothed feature encoder outputs the expectation of feature representations over the Gaussian distribution $\mathcal{N}(\mathbf{x}, I)$.

Gaussian robustness score. Define $S_{\mathbf{x}_t}(\mathbf{x})$ as the score function that evaluates feature discrepancy between an input \mathbf{x} and a targeted example \mathbf{x}_t , which is:

$$S_{\mathbf{x}_t}(\mathbf{x}) = \frac{1}{2} \left(1 + \text{Cos}(f_e(\mathbf{x}), f_e(\mathbf{x}_t)) \right) \quad (4)$$

where $\text{Cos}(\cdot, \cdot)$ denotes the cosine similarity and $S_{\mathbf{x}_t}(\mathbf{x}) \in [0, 1]$. The Gaussian robustness score $\hat{S}(\mathbf{x})$ is defined as:

$$\begin{aligned} \hat{S}(\mathbf{x}) &= \mathbb{E}_{\boldsymbol{\varepsilon} \sim \mathcal{N}(0, I)} [S_{\mathbf{x}}(\mathbf{x} + \boldsymbol{\varepsilon})] \\ &= \frac{1}{2} \left(1 + \mathbb{E}_{\boldsymbol{\varepsilon} \sim \mathcal{N}(0, I)} [\text{Cos}(f_e(\mathbf{x} + \boldsymbol{\varepsilon}), f_e(\mathbf{x}))] \right), \end{aligned} \quad (5)$$

The score $\hat{S}(\mathbf{x})$ evaluates the expected cosine similarity between the feature representation of a Gaussian-perturbed input $\mathbf{x} + \boldsymbol{\varepsilon}$ and that of the clean input \mathbf{x} , characterizing the Gaussian robustness of the vanilla feature encoder $f_e(\mathbf{x})$. Notably, we prove that this score $\hat{S}(\mathbf{x})$ preserves a good Lipschitz property, which serves as a theoretical foundation for proving the certified robustness for $\hat{f}_e(\mathbf{x})$.

Lemma 1 (Lipschitz property for the Gaussian robustness score). Let $\Phi(a) = \frac{1}{\sqrt{2\pi}} \int_{-\infty}^a \exp(-\frac{1}{2}s^2) ds$ be a standard Gaussian cumulative distribution function and Φ^{-1} be its inverse. For any feature encoder $f_e : \mathbf{x} \rightarrow \mathbf{z}$, the mapping $\mathbf{x} \rightarrow \Phi^{-1}(\hat{S}(\mathbf{x}))$ is $1 - \text{Lipschitz}$.

The proof of Lemma 1 is in the supplementary material, Section S.1. It implies that the mapping from \mathbf{x} to $\Phi^{-1}(\hat{S}(\mathbf{x}))$ exhibits strong adversarial robustness, as it satisfies a 1-Lipschitz constraint. Generally, $\hat{S}(\mathbf{x})$ measures the Gaussian robustness of the vanilla feature encoder $f_e(\mathbf{x})$. We then prove that **this score $\hat{S}(\mathbf{x})$ fundamentally determines the value of the certified robustness bound of its smoothed encoder $\hat{f}_e(\mathbf{x})$** . The following Theorem establishes an explicit relationship between this score and the lower bound on the adversarial feature cosine similarity.

Theorem 1 (Certified lower bound on the adversarial feature cosine similarity). For any feature encoder f_e and its smoothed version \hat{f}_e , let \mathbf{x} and \mathbf{x}' be clean and adversarial inputs with $\|\mathbf{x}' - \mathbf{x}\| \leq \epsilon$. The cosine similarity between

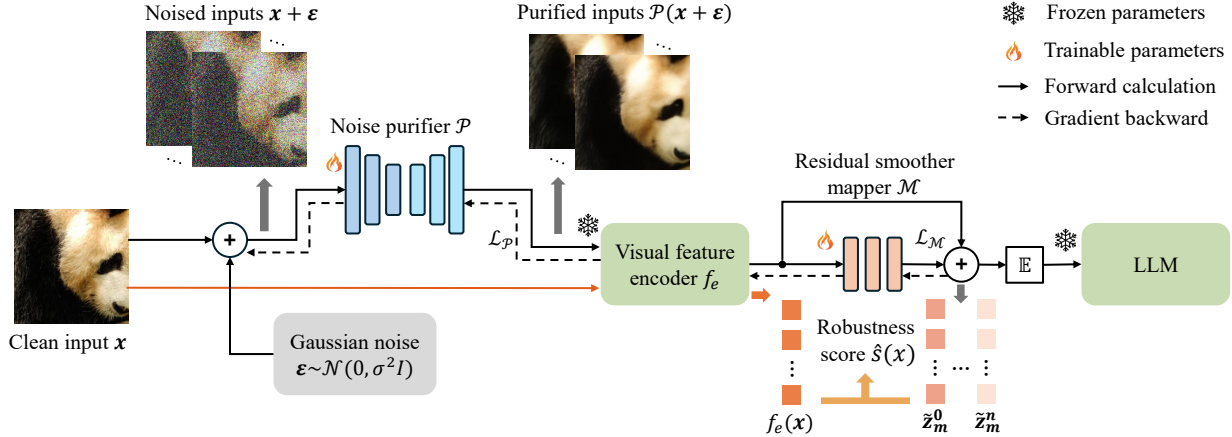


Figure 2. The training framework of the PSM. The purifier performs pre-processing and the smoothness mapper refines post-extracted features to enhance the Gaussian robustness. Parameters of MLLMs are frozen, and the purifier and mapper are optimized with \mathcal{L}_P and \mathcal{L}_M . For evaluation, the input x is replaced with adversarial input x' and the forward calculation marked by orange color will be removed.

the adversarial feature $\hat{f}_e(x')$ and clean feature $f_e(x)$ satisfies: $\text{Cos}(\hat{f}_e(x'), f_e(x)) \geq 2\Phi(\Phi^{-1}(\hat{S}(x)) - \epsilon) - 1$. Denote $2\Phi(\Phi^{-1}(\hat{S}(x)) - \epsilon) - 1$ as the Feature Cosine Similarity Bound (FCSB). Theorem 1 reveals that:

- By FS, we can turn any given feature encoder f_e into a smoothed version \hat{f}_e that maintains a FCSB between the adversarial and clean feature representations.
- By maximizing the robustness score $\hat{S}(x)$ of the given feature encoder f_e , we can effectively enhance the value of FCSB derived on its smoothed version \hat{f}_e .

The proof of Theorem 1 is in the supplementary material, Section S.1.

Corollary 1 (Certified radius \mathcal{R} for adversarial cosine similarity ≥ 0.5). Let x be the clean input, and x' be the adversarial input. Then $\text{Cos}(\hat{f}_e(x'), f_e(x)) \geq 0.5$, for all x' with $\|x' - x\|_2 \leq \mathcal{R}$, where:

$$\mathcal{R} = \Phi^{-1}(\hat{S}(x)) - \Phi^{-1}(0.75). \quad (6)$$

Building upon Theorem 1, Corollary 1 establishes a certified radius \mathcal{R} for the smoothed feature encoder. For any adversarial perturbation satisfying $\|\delta\|_2 \leq \mathcal{R}$, the FCSB of the smoothed encoder is guaranteed to remain above 0.5.

Why feature-space smoothing for MLLMs? Unlike previous smoothing methods, performing smoothing in the feature space offers several advantages:

- **Efficiency:** Compared to the previous RS that smooths the entire model \mathcal{F} , smoothing the feature encoder f_e , which is substantially lighter than the whole MLLM \mathcal{F} , significantly reduces the computational time of multiple forward calculations required by smoothing.
- **Generality:** The FS provides certified robustness at the feature representation level, making it applicable to various downstream tasks (e.g. image captioning, classification and visual question answering).

- **Effectiveness:** Since feature representations play a critical role in the final prediction, guaranteeing a trustworthy feature representation effectively improves the prediction reliability and robustness under adversarial attacks.

4. Purifier and Smoothness Mapper

Theorem 1 and Corollary 1 reveal an intriguing robustness property of the smoothed feature encoder \hat{f}_e . However, MLLMs' feature encoders f_e generally exhibits limited Gaussian robustness, which restricts the value of FCSB derived on \hat{f}_e . One solution is to estimate the smoothness score $\hat{S}(x)$ through Monte Carlo sampling and training f_e to maximize this score via gradient backpropagation. However, this could *reduce the adaptability and practicality of our FS protection, as fine-tuning and re-aligning the LLM with multi-modal feature encoders is highly complex and costly*. This thereby motivates us to propose the Purifier and Smoothness Mapper (PSM), a plug-and-play module that can be seamlessly integrated with MLLMs to enhance its Gaussian robustness score $\hat{S}(x)$.

The training framework of our proposed PSM is shown in Figure 2. The purifier P operates before feature extraction to denoise the Gaussian perturbations, and the smoothness mapper M performs post-extraction to do the feature refinement. Those two modules work together to enhance the Gaussian robustness of the given feature encoder.

4.1. Noise purifier

To denoise the Gaussian noise, P is trained to minimize the reconstruction loss l_{mse} , defined as:

$$l_{mse} = \mathbb{E}_{x \sim \mathcal{D}, \epsilon \sim \mathcal{N}(0, \sigma^2 I)} \|x - \mathcal{P}(x + \epsilon)\|, \quad (7)$$

where \mathcal{D} represents the data distribution. Meanwhile, to further enhance robustness score after plugging P , we also introduce a robustness loss l_{rb}^P , defined as:

$$l_{\text{rb}}^{\mathcal{P}} = \mathbb{E}_{\mathbf{x} \sim \mathcal{D}, \mathbf{\epsilon} \sim \mathcal{N}(0, \sigma^2 I)} [\text{Cos}(f_e(\mathcal{P}(\mathbf{x} + \mathbf{\epsilon})), f_e(\mathbf{x}))], \quad (8)$$

which encourages feature consistency between the purified and clean representations. Practically, we adopt the ImageNet-pretrained guided-diffusion [7] as our purifier \mathcal{P} and perform one-step diffusion for denoising in our main experiments. We then fine-tune this model on the dataset \mathcal{D} using the purifier loss $\mathcal{L}_{\mathcal{P}}$, which is:

$$\mathcal{L}_{\mathcal{P}} = l_{\text{diff}} + \lambda_1 l_{\text{rb}}^{\mathcal{P}} + \lambda_2 l_{\text{mse}}, \quad (9)$$

where l_{diff} denotes the original diffusion loss, and λ_1 and λ_2 are the weighting coefficients. More details of the fine-tuning process on \mathcal{P} can be found in the supplementary material, Section S.2.

4.2. Residual smoothness mapper

For the residual smoothness mapper \mathcal{M} , we utilize a noise-aware residual module to enhance feature robustness while preserving its statistical distribution. The main process of this mapper can be formulated as:

$$\tilde{\mathbf{z}}_m = \tilde{\mathbf{z}} + \mathcal{M}(\tilde{\mathbf{z}}, \sigma) = \tilde{\mathbf{z}} + \sum_{i=0}^{k-1} m_i(\tilde{\mathbf{z}}_i, \sigma), \quad (10)$$

where $\tilde{\mathbf{z}} = f_e(\mathcal{P}(\mathbf{x} + \mathbf{\epsilon}))$ denotes the purified feature representations and $\tilde{\mathbf{z}}_{i+1} = m_i(\tilde{\mathbf{z}}_i, \sigma)$ is the intermediate output with $\tilde{\mathbf{z}}_0 = \tilde{\mathbf{z}}$. σ is the noise strength that adaptively controls the output magnitude of the mapper. k is the number of blocks ($k = 3$ in our experiments unless otherwise specified), and each block $m_i(\cdot)$ contains multi-head attention, depthwise convolution, and MLP branches to refine the purified representation. To enhance the Gaussian robustness of the refined representation, we introduce the mapper robustness loss $l_{\text{rb}}^{\mathcal{M}}$, defined as:

$$l_{\text{rb}}^{\mathcal{M}} = \mathbb{E}_{\mathbf{x} \sim \mathcal{D}, \mathbf{\epsilon} \sim \mathcal{N}(0, \sigma^2 I)} [\text{Cos}(\tilde{\mathbf{z}}_m, f_e(\mathbf{x}))], \quad (11)$$

which encourages feature consistency between the refined and clean representations. Meanwhile, to ensure that the refined feature preserves the statistical characteristics of the clean feature, we introduce two regularization terms: the identical loss l_{id} and the statistical loss l_{stats} , defined as:

$$\begin{cases} l_{\text{stats}} = \mathbb{E}_{\mathbf{x} \sim \mathcal{D}, \mathbf{\epsilon} \sim \mathcal{N}(0, \sigma^2 I)} \frac{1}{D} \sum_{d=1}^D [(\mu_{\tilde{\mathbf{z}}_m}^{(d)} - \mu_{\mathbf{z}}^{(d)})^2 + (\sigma_{\tilde{\mathbf{z}}_m}^{(d)} - \sigma_{\mathbf{z}}^{(d)})^2], \\ l_{\text{id}} = \mathbb{E}_{\mathbf{x} \sim \mathcal{D}} \|\mathcal{M}(\tilde{\mathbf{z}}, 0)\|_2^2. \end{cases} \quad (12)$$

where $\tilde{\mathbf{z}}_m, \mathbf{z} \in \mathbb{R}^{B \times L \times D}$ with batch size B , token number L and feature dimension D . The l_{stats} enforces consistency between the element-wise mean μ^d and standard deviation σ^d of two representations, thereby preserving the statistical characteristics. Meanwhile, the identity loss l_{id} constrains the mapping network \mathcal{M} when the noise strength $\sigma = 0$, promoting stability and preventing undesired distortions on clean inputs. The overall training loss $\mathcal{L}_{\mathcal{M}}$ is defined as:

Algorithm 1 Training algorithm of PSM

```

1: Input: dataset  $\mathcal{D}$ , feature encoder  $f_e$ , purifier  $\mathcal{P}$ , mapper  $\mathcal{M}$ , sampling number  $n_0$ , noise standard deviation  $\sigma$ , and loss weights  $\lambda_1, \lambda_2, \lambda_3, \lambda_4$ .
2: Output: trained purifier  $\mathcal{P}$  and mapper  $\mathcal{M}$ .
3: // Stage 1: Fine-tune the purifier  $\mathcal{P}$ 
4: for each batch  $\mathbf{x} \sim \mathcal{D}$  do
5:    $\mathbf{z} = f_e(\mathbf{x})$ 
6:   for  $i = 1, \dots, n_0$  do
7:     Sample  $\mathbf{\epsilon}^i \sim \mathcal{N}(0, \sigma^2 I)$ 
8:      $\tilde{\mathbf{x}}^i = \mathcal{P}(\mathbf{x} + \mathbf{\epsilon}^i)$ , and  $\tilde{\mathbf{z}}^i = f_e(\tilde{\mathbf{x}}^i)$ 
9:     Compute  $l_{\text{rb}}^{\mathcal{P}}$  and  $l_{\text{mse}}$  using Equations 7, 8.
10:    Update  $\mathcal{P}$  by gradient descent on  $\nabla_{\mathcal{P}} \mathcal{L}_{\mathcal{P}}$ 
11: // Stage 2: Train the smoothness mapper  $\mathcal{M}$ 
12: for each batch  $\mathbf{x} \sim \mathcal{D}$  do
13:    $\mathbf{z} = f_e(\mathbf{x})$ 
14:   for  $i = 1, \dots, n_0$  do
15:     Sample  $\mathbf{\epsilon}^i \sim \mathcal{N}(0, \sigma^2 I)$ 
16:      $\tilde{\mathbf{x}}^i = \mathcal{P}(\mathbf{x} + \mathbf{\epsilon}^i)$ , and  $\tilde{\mathbf{z}}_m^i = f_e(\tilde{\mathbf{x}}^i) + \mathcal{M}(\tilde{\mathbf{z}}^i, \sigma)$ 
17:     Compute  $l_{\text{rb}}^{\mathcal{M}}$ ,  $l_{\text{id}}$  and  $l_{\text{stats}}$  using Equations 11, 12.
18:     Update  $\mathcal{M}$  by gradient descent on  $\nabla_{\mathcal{M}} \mathcal{L}_{\mathcal{M}}$ 

```

$$\mathcal{L}_{\mathcal{M}} = l_{\text{rb}}^{\mathcal{M}} + \lambda_3 l_{\text{stats}} + \lambda_4 l_{\text{id}}, \quad (13)$$

where λ_3 and λ_4 are the weighting coefficients. More details of the training process on the residual smoothness mapper can be found in the supplementary material, Section S.2.

4.3. Further discussion on PSM

Certified robustness for the encoder f_e with PSM. Let f'_e denote the feature encoder integrated with the proposed PSM. Then the forward process can be formulated as:

$$f'_e(\mathbf{x} + \mathbf{\epsilon}) = f_e(\mathcal{P}(\mathbf{x} + \mathbf{\epsilon})) + \mathcal{M}(\tilde{\mathbf{z}}, \sigma). \quad (14)$$

Under this condition, the smoothed feature encoder and smoothness score are defined as:

$$\begin{aligned} \hat{f}'_e(\mathbf{x}) &= \frac{1}{(2\pi)^{d/2}} \int_{\mathbb{R}^d} f'_e(\mathbf{x} + \mathbf{\epsilon}) \exp(-\frac{1}{2}\|\mathbf{\epsilon}\|^2) d\mathbf{\epsilon}, \\ \hat{S}'(\mathbf{x}) &= \frac{1}{2} \left(1 + \mathbb{E}_{\mathbf{\epsilon} \sim \mathcal{N}(0, \sigma^2 I)} [\text{Cos}(f'_e(\mathbf{x} + \mathbf{\epsilon}), f_e(\mathbf{x}))] \right), \end{aligned} \quad (15)$$

Where $\hat{S}'(\mathbf{x}) \in [0, 1]$. We can prove that the Lipschitz property derived in Lemma 1 still holds, and the theoretical bound in Section 3 remains valid. Then, utilizing Theorem 1 and Corollary 1, we can derive the certified lower bound on $\text{Cos}(\hat{f}'_e(\mathbf{x}'), f_e(\mathbf{x}))$ for any adversarial input \mathbf{x}' .

Training algorithm and dataset construction. The training procedure of PSM is summarized in Algorithm 1, where the purifier \mathcal{P} and the smoothness mapper \mathcal{M} are trained sequentially via a two-stage manner. The expectation over Gaussian perturbations is approximated by Monte Carlo sampling with n_0 samples drawn from $\mathcal{N}(0, \sigma^2 I)$, where we set $n_0 = 8$ in our training to balance efficiency and estimation accuracy. Notably, all modules can be trained in a

Table 1. Experimental results on adversarial robustness of different defense methods and MLLMs on image captioning tasks. Values in parentheses denote the average textual similarity measured by GPTScore. The overall best results are shown in **bold**, and the best results without smoothing are underlined, highlighting the significant performance gain introduced by our proposed FS-PSM.

Model	Method	M-Attack [23]			FOA [14]			AttackVLM [51]		
		FCS \uparrow	ACC \uparrow	ASR \downarrow	FCS \uparrow	ACC \uparrow	ASR \downarrow	FCS \uparrow	ACC \uparrow	ASR \downarrow
LLaVA-1.5-7B	Org.	0.385	1% (0.06)	93% (0.54)	0.388	1% (0.049)	94% (0.578)	0.430	3% (0.089)	88% (0.490)
	Smoothed org.	0.650	82% (0.694)	2% (0.028)	0.652	87% (0.735)	1% (0.021)	0.660	89% (0.727)	2% (0.018)
	FARE [37]	0.588	44% (0.409)	24% (0.097)	0.504	19% (0.197)	51% (0.222)	0.499	18% (0.190)	44% (0.221)
	Smoothed FARE	0.716	59% (0.501)	14% (0.069)	0.656	35% (0.327)	29% (0.153)	0.729	60% (0.503)	11% (0.061)
	TeCoA [29]	0.720	51% (0.458)	16% (0.081)	0.674	21% (0.236)	37% (0.187)	0.606	17% (0.179)	43% (0.218)
	Smoothed TeCoA	0.805	59% (0.498)	14% (0.056)	0.789	39% (0.364)	20% (0.094)	0.755	42% (0.358)	18% (0.104)
Open Flamingo-9B	Org.	0.351	1% (0.089)	86% (0.583)	0.347	1% (0.091)	87% (0.569)	0.442	16% (0.222)	59% (0.379)
	Smoothed org.	0.673	73% (0.655)	1% (0.063)	0.672	69% (0.623)	0% (0.061)	0.703	73% (0.687)	0% (0.055)
	FARE [37]	0.588	36% (0.407)	17% (0.145)	0.504	20% (0.249)	40% (0.240)	0.499	15% (0.243)	40% (0.247)
	Smoothed FARE	0.716	55% (0.529)	9% (0.088)	0.656	40% (0.414)	17% (0.125)	0.729	50% (0.488)	4% (0.089)
	TeCoA [29]	0.720	51% (0.472)	13% (0.116)	0.674	21% (0.240)	30% (0.210)	0.606	19% (0.244)	34% (0.225)
	Smoothed TeCoA	0.805	56% (0.518)	5% (0.090)	0.789	50% (0.454)	8% (0.095)	0.755	38% (0.398)	12% (0.126)

self-supervised fashion, without relying on task-specific labels. Thus, to promote generalization across diverse visual domains and ensure compatibility with various MLLMs’ downstream tasks, we collect the training dataset \mathcal{D} comprising 5,000 images from heterogeneous domains, including medical, cartoon, and natural images.

Table 2. The average FCSB at different predetermined adversarial bounds ϵ and the average certified radius \mathcal{R} for $\text{FCSB} \geq 0.5$.

Encoder	σ	Avg. FCSB at different adv-bound ϵ					Avg. \mathcal{R}
		0.125	0.25	0.375	0.50	0.75	
CLIP-B16	0.25	0.828	0.623	0.313	-0.06	/	0.31
CLIP-B16+ \mathcal{P} & \mathcal{M}	0.25	0.975	0.920	0.789	0.553	/	0.53
CLIP-B16	0.50	0.717	0.586	0.439	0.253	-0.132	0.33
CLIP-B16+ \mathcal{P} & \mathcal{M}	0.50	0.970	0.945	0.907	0.846	0.649	0.89

Certified robustness bound of FS-PSM. To evaluate the effectiveness of the proposed PSM module, we adopt CLIP-B16 [33] as the vanilla feature encoder f_e and assess the certified robustness bound of both the original smoothed encoder \hat{f}_e and its PSM-enhanced counterpart \hat{f}'_e under the FS. We report both the certified FCSB under different adversarial constraints ϵ and the certified radius \mathcal{R} for $\text{FCSB} \geq 0.5$. The results are shown in Table 2. For implementation, we randomly sample 100 images from the ImageNet dataset [6] and approximate the Gaussian expectation using $n = 1,000$ Monte Carlo samples. As shown in Table 2, integrating PSM consistently enhances both the certified FCSB across a range of perturbation magnitudes and the average certified radius \mathcal{R} , indicating substantial improvements in certified robustness. To further assess the practical protection of our FS-PSM, we then conduct extensive experiments across multiple MLLMs and downstream tasks in the next section, evaluating their performance before and after smoothing under various strong white-box attacks.

5. Experiments

5.1. Experimental setup

Evaluated models and tasks. Since the proposed FS requires access to the forward feature computation process of MLLMs, we primarily validate its effectiveness on open-sourced MLLMs, including LLaVA-V1.5-7B [24, 25] and OpenFlamingo9B [1]. We comprehensively assess the performance of plugging the FS-PSM under adversarial conditions across multiple downstream tasks, including:

- Image captioning:** Following the setup in [14, 23], we randomly take 100 images from the NIPS 2017 Adversarial Attacks and Defenses Competition dataset ¹ and ask the model to caption the image.
- Image Classification:** We randomly sample 500 images from 10 classes in the ImageNet dataset [6] and ask the model to classify the input.
- Visual Question Answering (VQA):** We utilize 100 image-question pairs from the ScienceQA dataset [26]. Meanwhile, we also evaluate our FS-PSM on the original CLIP-L14 [33] on image classification for the generality.
- The threat model.** To comprehensively assess the robustness under strong adversaries, we employ three SOTA adversarial attacks specifically designed for MLLMs, named AttackVLM [51], M-Attack [23], and FOA [14] using **the white-box setting**. All attacks are implemented following their original best configurations, with the adversarial perturbation budget ϵ set to $\|\epsilon\|_\infty = 16/255$. We also consider a stronger bound with $\|\epsilon\|_\infty = 32/255$ for a stress test.
- Compared defense methods.** As this work pioneers the research for MLLMs’ certified robustness, we primarily compare our defense with adversarial training based approaches, namely FARE [37] and TeCoA [29]. Both FARE and TeCoA adopt adversarial training to obtain robust fea-

¹<https://nips.cc/Conferences/2017/CompetitionTrack>

Table 3. Experimental results on adversarial robustness of different defense methods and MLLMs on image classification tasks. The overall best results are shown in **bold**, and the best results without smoothing are underlined.

Model	Method	M-Attack [23]			FOA [14]			AttackVLM [51]		
		FCS↑	ACC↑	ASR↓	FCS↑	ACC↑	ASR↓	FCS↑	ACC↑	ASR↓
LLaVA-1.5-7B	Org.	0.427	8.2%	78.2%	0.437	3.8 %	81.0 %	0.458	6.0%	78.4%
	Smoothed org.	0.681	90.4%	0.6%	0.697	88.8%	0.4%	0.700	88.4%	0.2%
	FARE [37]	0.574	55.4%	14.6%	0.521	24.8%	39.8%	0.508	25.8%	45.0%
	Smoothed FARE	0.859	75.6%	5.2%	0.712	72.0%	5.6%	0.699	74.0%	6.2%
	TeCoA [29]	0.731	<u>67.4%</u>	<u>2%</u>	0.626	<u>29.0%</u>	<u>20.0%</u>	0.592	<u>33.6%</u>	<u>17.8%</u>
	Smoothed TeCoA	0.819	74.4%	0.4%	0.727	57.2%	3.0%	0.711	57.4%	2.0%
CLIP-L14	Org.	0.427	18.0%	37.2%	0.437	10.0 %	52.4 %	0.458	16.0%	48.4%
	Smoothed org.	0.681	92.4%	0.4%	0.697	92.0%	0.4%	0.700	92.0%	0.4%
	FARE [37]	0.574	70.4%	5.2%	0.521	<u>42.0%</u>	<u>14.4%</u>	0.508	35.6%	24.4%
	Smoothed FARE	0.859	85.2%	0.8%	0.712	81.6%	0%	0.699	82.4%	0%
	TeCoA [29]	0.731	<u>81.2%</u>	<u>2.4%</u>	0.626	39.2%	20.2%	0.592	<u>35.8%</u>	<u>24.4%</u>
	Smoothed TeCoA	0.819	88.4%	1.6%	0.727	76.0%	4.8%	0.711	73.2%	6.0%

ture encoders that can be directly integrated into models such as LLaVA-1.5-7B and OpenFlamingo-9B. To ensure a fair and consistent comparison, we obtain all adversarially trained feature encoders from their official repositories, without any modification.

Implementation details. For practical inference efficiency, we set the number of samples to $n_0 = 4$ for smoothing, which provides a favorable trade-off between robustness and runtime. We train three independent PSM modules, utilizing the vanilla feature encoders from models including LLaVA-1.5-7B, OpenFlamingo-9B, and CLIP-L14. To further assess cross-model generalization, we evaluate the PSM trained on a vanilla encoder by directly applying it to adversarially trained encoders FARE and TeCoA. For all feature encoders, we set hyperparameters $\lambda_1, \lambda_2, \lambda_4 = 0.25$, $\lambda_3 = 100$, and $\sigma = 0.25$. In our tables, the term "smoothed" denotes the process of smoothing the encoder via FS and enhancing it with PSM.

Evaluation metrics. We mainly report: the Feature Cosine Similarity (**FCS**), the Accuracy (**ACC**), and the Attack Success Rate (**ASR**). Specifically, FCS measures the cosine similarity between clean and adversarial features extracted **by the same feature encoder**, reflecting its feature-space robustness. ACC denotes the proportion of correctly completed tasks, while ASR indicates the proportion of cases where the model is successfully manipulated to produce the adversarially targeted outputs. For image classification and VQA tasks, ACC and ASR are determined by whether the MLLM outputs match the correct or adversarial targets.

For image captioning, following [23], we adopt the LLM-as-a-judge protocol [52] to evaluate ACC and ASR. Specifically, we first generate the clean and adversarially targeted captions by feeding the clean and targeted inputs into the vanilla MLLM (*e.g.*, the original LLaVA). We then obtain the predicted caption by feeding the adversarially perturbed input into the tested model (*e.g.*,

Smoothed LLaVA). The textual similarity is computed using GPTScore [9], where a task is considered successful if the GPTScore between the **predicted and clean captions** is ≥ 0.5 , and an attack is considered successful if the GPTScore between the predicted and **adversarially targeted captions** is ≥ 0.3 .

5.2. Experimental results on different tasks

Image captioning. The comparative results of different defense methods and MLLMs on the image captioning task are presented in Table 1. In this task, the adversaries aim to manipulate the MLLMs into producing the caption corresponding to a completely unrelated and maliciously chosen target image. These results demonstrate that converting MLLMs into their smoothed variants via the proposed FS-PSM yields **consistently strong robustness** across diverse adversarial attacks, while empirical defenses exhibit a noticeable performance drop under stronger attacks. When adversaries vary from M-Attack to FOA, the accuracy of **LLaVA with FARE drops from 44% to 19%, and that of TeCoA declines from 51% to 21%**. Notably, utilizing FS-PSM achieves remarkable improvements, with the **accuracy of LLaVA increasing from 1% to 87% and the ASR dropping from 94% to 1%** under the strongest FOA attack. Furthermore, the results demonstrate that FS-PSM possesses strong cross-model generalization; directly integrating it into FARE and TeCoA without any fine-tuning consistently enhances their robustness.

Image classification. The comparative results of different defense methods on the image classification are presented in Table 3. The adversarial objective is to mislead the model into classifying an adversarial image into a maliciously targeted class that is semantically unrelated to the original one. For image classification with CLIP-L14, we train a one-layer classification head on top of its extracted features. The results indicate that FS-PSM provides consis-

Table 4. Experimental results on adversarial robustness of different defense methods and MLLMs on VQA tasks. The overall best results are shown in **bold**, and the best results without smoothing are underlined.

Model	Method	M-Attack [23]			FOA [14]			AttackVLM [51]		
		FCS↑	ACC↑	ASR↓	FCS↑	ACC↑	ASR↓	FCS↑	ACC↑	ASR↓
LLaVA-1.5-7B	Org.	0.398	31%	28%	0.383	22%	22%	0.474	25%	27%
	Smoothed org.	0.732	47%	0%	0.676	43%	0%	0.765	43%	1%
	FARE [37]	0.657	47%	5%	0.590	<u>32%</u>	0%	0.550	<u>38%</u>	7%
	Smoothed FARE	0.859	48%	1%	0.768	38%	0%	0.818	39%	0%
	TeCoA [29]	0.788	31%	<u>2%</u>	0.748	31%	2%	0.667	31%	1%
	Smoothed TeCoA	0.917	32%	1%	0.858	34%	1%	0.862	29%	1%

tent and substantial robustness improvements for classification tasks. Meanwhile, those adversarial training-based defenses exhibit a noticeable performance drop under strong FOA attacks. The accuracy of **FARE with LLaVA drops from 55.4% to 24.8%, and that of TeCoA declines from 67.4% to 29.0%** when adversaries vary from M-Attack to FOA. Integrating FS-PSM into the vanilla model achieves remarkable improvements, with **the accuracy of LLaVA increasing from 3.8% to 88.0% and the ASR dropping from 81% to 0.4%** under the strongest FOA attack. Meanwhile, directly integrating the FS-PSM brings huge robustness gains for those adversarially trained feature encoders. **VQA.** The comparative results of different defense methods on LLaVA-1.5-7B on the VQA are presented in Table 4. The performances of OpenFlamingo and CLIP are omitted, as these models are not directly applicable to the VQA task. In this setting, the adversarial objective is to mislead the model into selecting a wrong option, “*None of the above*”, for each image–question pair. This task presents a greater challenge for pure vision-based adversaries than the previous two, as MLLMs can often infer correct answers directly from textual cues without relying heavily on visual inputs. The results demonstrate that incorporating our method yields substantial performance improvements across all attack types, significantly enhancing prediction accuracy while reducing the attack success rate to nearly zero. More implementation details for the main results are presented in our supplementary material, section S.3.

5.3. Further analysis on the main results

Reasons for FARE and TeCoA performing poorly with high FCS. Although those encoders preserve high FCS with respect to their clean inputs, the adversarial training process inherently induces a distributional shift in the feature representations. Subsequent adversarial perturbations further amplify this shift, leading to more pronounced performance degradation. In addition, the limited diversity of adversarial training data restricts their feature generalization ability, amplifying the performance drop when evaluated on downstream tasks with unseen or mismatched data distributions.

Advantages of our proposed FS with PSM. The experimental results highlight three key advantages: (1) **Effectiveness:**

Table 5. The ablation study. We report the average FCSB and the average \mathcal{R} for $\text{FCSB} \geq 0.5$ for certified robustness. We report the average accuracy and ASR for empirical robustness under FOA attack. The clean accuracy without attack is **92.4%**.

Encoder	σ	Avg. FCSB at different ϵ			Avg. \mathcal{R}	Acc	ASR
		0.25	0.50	0.75			
CLIP-B16	/	/	/	/	/	1.6%	95.6%
FS	CLIP-B16	0.586	0.253	-0.132	0.33	42.4%	0.8%
	CLIP-B16+ \mathcal{M}	0.884	0.717	0.436	0.71	66.8%	0.4%
	CLIP-B16+ \mathcal{P} & \mathcal{M}	0.970	0.907	0.846	0.89	91.6%	0.4%

Effectiveness: utilizing the proposed FS-PSM substantially enhances the performance of various MLLMs under adversarial attacks; (2) **Trustworthiness:** compared with adversarial training, FS-PSM provides more stable and consistently stronger protection across a wide range of attacks; (3) **Generality:** FS-PSM can be combined with other defenses to enhance the effectiveness without additional fine-tuning.

5.4. Ablation study

To rigorously assess the contribution of the proposed FS and each module of PSM, we adopt CLIP-B16 as the base feature encoder and evaluate the performance on the image classification task. We report both the theoretically certified robustness and the empirical performance under the strong FOA attack. The results are summarized in Table 5, where the first row indicates the performance of the vanilla CLIP-B16 model without utilizing the FS. The next three rows are the results of the smoothed CLIP-B16 with FS, smoothed CLIP-B16 with FS and mapper \mathcal{M} , and smoothed CLIP-B16 with FS and PSM. The results demonstrate that enforcing smoothness in the feature space substantially enhances practical robustness against adversarial perturbations, raising the accuracy from 1.6% to 91.6% and reducing the ASR from 95.6% to 0.4%. Meanwhile, each component makes a significant contribution to improving both the certified radius \mathcal{R} and adversarial robustness.

More experimental results on: 1) the performance of using different purifier (a lightweight U-Net denoiser), 2) the performance under a stronger adversarial bound $\|\epsilon\|_\infty = 32$, and 3) efficiency–robustness trade-off under various n_0 , are provided in our supplementary material, section S.3.

6. Conclusion.

This work pioneers the research on establishing the certified robustness of MLLMs via a feature-space perspective. By introducing the Feature-space Smoothing (FS) framework, we show how to transform any feature encoder into a smoothed version that is equipped with a theoretical lower bound on the cosine similarity between clean and adversarial representations. Moreover, we introduce the Purifier and Smoothness Mapper (PSM), a plug-and-play module that can be seamlessly integrated into existing MLLMs to amplify the certified robustness under FS without any fine-tuning. Extensive experiments demonstrate that the proposed FS-PSM not only provides strong theoretical robustness guarantees but also achieves superior empirical protection against various attacks.

References

[1] Anas Awadalla, Irena Gao, Josh Gardner, Jack Hessel, Yusuf Hanafy, Wanrong Zhu, Kalyani Marathe, Yonatan Bitton, Samir Gadre, Shiori Sagawa, et al. Openflamingo: An open-source framework for training large autoregressive vision-language models. *arXiv preprint arXiv:2308.01390*, 2023. 6

[2] Stephen Casper, Lennart Schulze, Oam Patel, and Dylan Hadfield-Menell. Defending against unforeseen failure modes with latent adversarial training. *arXiv preprint arXiv:2403.05030*, 2024. 1, 2

[3] Bin Chen, Jiali Yin, Shukai Chen, Bohao Chen, and Ximeng Liu. An adaptive model ensemble adversarial attack for boosting adversarial transferability. In *CVPR*, 2023. 1, 2

[4] Jeremy Cohen, Elan Rosenfeld, and Zico Kolter. Certified adversarial robustness via randomized smoothing. In *ICML*, 2019. 1, 2

[5] Xuanming Cui, Alejandro Aparcero, Young Kyun Jang, and Ser-Nam Lim. On the robustness of large multimodal models against image adversarial attacks. In *CVPR*, 2024. 1, 2

[6] Jia Deng, Wei Dong, Richard Socher, Li-Jia Li, Kai Li, and Li Fei-Fei. Imagenet: A large-scale hierarchical image database. In *CVPR*, 2009. 6

[7] Prafulla Dhariwal and Alexander Nichol. Diffusion models beat gans on image synthesis. *NeurIPS*, 2021. 5

[8] Xinlong Ding, Jiansheng Chen, Hongwei Yu, Yu Shang, Yingning Qin, and Huimin Ma. Transferable adversarial attacks for object detection using object-aware significant feature distortion. In *AAAI*, 2024. 3

[9] Jinlan Fu, See Kiong Ng, Zhengbao Jiang, and Pengfei Liu. Gptscore: Evaluate as you desire. In *Proceedings of the 2024 Conference of the North American Chapter of the Association for Computational Linguistics: Human Language Technologies*, 2024. 7

[10] Ian J Goodfellow, Jonathon Shlens, and Christian Szegedy. Explaining and harnessing adversarial examples. *arXiv preprint arXiv:1412.6572*, 2014. 1

[11] Zhongkai Hao, Chengyang Ying, Yinpeng Dong, Hang Su, Jian Song, and Jun Zhu. Gsmooth: Certified robustness against semantic transformations via generalized randomized smoothing. In *ICML*, 2022. 2

[12] Matthias Hein and Maksym Andriushchenko. Formal guarantees on the robustness of a classifier against adversarial manipulation. *NeurIPS*, 2017. 1

[13] Qian Huang, Isay Katsman, Horace He, Zeqi Gu, Serge Belongie, and Ser-Nam Lim. Enhancing adversarial example transferability with an intermediate level attack. In *ICCV*, 2019. 3

[14] Xiaojun Jia, Sensen Gao, Simeng Qin, Tianyu Pang, Chao Du, Yihao Huang, Xinfeng Li, Yiming Li, Bo Li, and Yang Liu. Adversarial attacks against closed-source mllms via feature optimal alignment. *NeurIPS*, 2025. 1, 2, 3, 6, 7, 8, 13, 14

[15] Kazuya Kakizaki, Kazuto Fukuchi, and Jun Sakuma. Certified defense for content based image retrieval. In *CVPR*, 2023. 2

[16] Mathias Lecuyer, Vaggelis Atlidakis, Roxana Geambasu, Daniel Hsu, and Suman Jana. Certified robustness to adversarial examples with differential privacy. In *2019 IEEE symposium on security and privacy (SP)*, 2019. 2

[17] Chun Tong Lei, Hon Ming Yam, Zhongliang Guo, Yifei Qian, and Chun Pong Lau. Instant adversarial purification with adversarial consistency distillation. In *CVPR*, 2025. 2

[18] B Li, C Chen, W Wang, and L Carin. Second-order adversarial attack and certifiable robustness. *arXiv preprint arXiv:1809.03113*, 2018. 2

[19] Junnan Li, Dongxu Li, Silvio Savarese, and Steven Hoi. Blip-2: Bootstrapping language-image pre-training with frozen image encoders and large language models. In *ICML*, 2023. 2

[20] Qizhang Li, Yiwen Guo, and Hao Chen. Yet another intermediate-level attack. In *ECCV*, 2020. 3

[21] Qizhang Li, Yiwen Guo, Wangmeng Zuo, and Hao Chen. Improving adversarial transferability via intermediate-level perturbation decay. *NeurIPS*, 2023. 3

[22] Xiao Li, Wenxuan Sun, Huanran Chen, Qiongxu Li, Yingzhe He, Jie Shi, and Xiaolin Hu. ADBM: Adversarial diffusion bridge model for reliable adversarial purification. In *ICLR*, 2025. 2

[23] Zhaoyi Li, Xiaohan Zhao, Dong-Dong Wu, Jiacheng Cui, and Zhiqiang Shen. A frustratingly simple yet highly effective attack baseline: Over 90% success rate against the strong black-box models of gpt-4.5/4o/o1. In *ICML 2025 Workshop on Reliable and Responsible Foundation Models*, 2025. 1, 2, 3, 6, 7, 8, 13

[24] Haotian Liu, Chunyuan Li, Qingyang Wu, and Yong Jae Lee. Visual instruction tuning. *NeurIPS*, 2023. 6

[25] Haotian Liu, Chunyuan Li, Yuheng Li, and Yong Jae Lee. Improved baselines with visual instruction tuning. In *CVPR*, 2024. 6

[26] Pan Lu, Swaroop Mishra, Tanglin Xia, Liang Qiu, Kai-Wei Chang, Song-Chun Zhu, Oyvind Tafjord, Peter Clark, and Ashwin Kalyan. Learn to explain: Multimodal reasoning via thought chains for science question answering. *NeurIPS*, 2022. 6

[27] Aleksander Madry, Aleksandar Makelov, Ludwig Schmidt, Dimitris Tsipras, and Adrian Vladu. Towards deep learning models resistant to adversarial attacks. In *ICLR*, 2018. 1, 2

[28] Hashmat Shadab Malik, Fahad Shamshad, Muzammal Naseer, Karthik Nandakumar, Fahad Khan, and Salman Khan. Robust-llava: On the effectiveness of large-scale robust image encoders for multi-modal large language models. *arXiv preprint arXiv:2502.01576*, 2025. 2

[29] Chengzhi Mao, Scott Geng, Junfeng Yang, Xin Wang, and Carl Vondrick. Understanding zero-shot adversarial robustness for large-scale models. In *ICLR*, 2023. 1, 2, 6, 7, 8, 13, 14

[30] Weili Nie, Brandon Guo, Yujia Huang, Chaowei Xiao, Arash Vahdat, and Animashree Anandkumar. Diffusion models for adversarial purification. In *ICML*, 2022. 2

[31] Xiangyu Qi, Kaixuan Huang, Ashwinee Panda, Peter Henderson, Mengdi Wang, and Prateek Mittal. Visual adversarial examples jailbreak aligned large language models. In *AAAI*, 2024. 2

[32] Yixiang Qiu, Hao Fang, Hongyao Yu, Bin Chen, MeiKang Qiu, and Shu-Tao Xia. A closer look at gan priors: Exploiting intermediate features for enhanced model inversion attacks. In *ECCV*, 2024. 3

[33] Alec Radford, Jong Wook Kim, Chris Hallacy, Aditya Ramesh, Gabriel Goh, Sandhini Agarwal, Girish Sastry, Amanda Askell, Pamela Mishkin, Jack Clark, et al. Learning transferable visual models from natural language supervision. In *ICML*, 2021. 2, 6

[34] Aditi Raghunathan, Jacob Steinhardt, and Percy Liang. Certified defenses against adversarial examples. In *ICLR*, 2018. 2

[35] Sylvestre-Alvise Rebuffi, Sven Gowal, Dan Andrei Calian, Florian Stimberg, Olivia Wiles, and Timothy A Mann. Data augmentation can improve robustness. *NeurIPS*, 2021. 1, 2

[36] Hadi Salman, Jerry Li, Ilya Razenshteyn, Pengchuan Zhang, Huan Zhang, Sebastien Bubeck, and Greg Yang. Provably robust deep learning via adversarially trained smoothed classifiers. *NeurIPS*, 2019. 2

[37] Christian Schlarbmann, Naman Deep Singh, Francesco Croce, and Matthias Hein. Robust clip: unsupervised adversarial fine-tuning of vision embeddings for robust large vision-language models. In *ICML*, 2024. 1, 2, 6, 7, 8, 13, 14

[38] Florian Tramer, Nicholas Carlini, Wieland Brendel, and Aleksander Madry. On adaptive attacks to adversarial example defenses. *NeurIPS*, 2020. 1, 2

[39] Yubo Wang, Chaohu Liu, Yanqiu Qu, Haoyu Cao, Deqiang Jiang, and Linli Xu. Break the visual perception: Adversarial attacks targeting encoded visual tokens of large vision-language models. In *ACM MM*, 2024. 2

[40] Zhibo Wang, Hengchang Guo, Zhifei Zhang, Wenxin Liu, Zhan Qin, and Kui Ren. Feature importance-aware transferable adversarial attacks. In *CVPR*, 2021. 3

[41] Zeyu Wang, Xianhang Li, Hongru Zhu, and Cihang Xie. Revisiting adversarial training at scale. In *CVPR*, 2024. 1, 2

[42] Zekai Wang, Zhengyu Zhou, and Weiwei Liu. Drf: Improving certified robustness via distributional robustness framework. In *AAAI*, 2024. 2

[43] Eric Wong and Zico Kolter. Provable defenses against adversarial examples via the convex outer adversarial polytope. In *ICML*, 2018. 2

[44] Kaiwen Wu, Allen Wang, and Yaoliang Yu. Stronger and faster wasserstein adversarial attacks. In *ICML*, 2020. 1, 2

[45] Sophie Xhonneux, Alessandro Sordoni, Stephan Günnemann, Gauthier Gidel, and Leo Schwinn. Efficient adversarial training in llms with continuous attacks. *NeurIPS*, 2024. 1, 2

[46] Song Xia, Wenhan Yang, Yi Yu, Xun Lin, Henghui Ding, Lingyu Duan, and Xudong Jiang. Transferable adversarial attacks on sam and its downstream models. *NeurIPS*, 2024. 3

[47] Song Xia, Yi Yu, Xudong Jiang, and Henghui Ding. Mitigating the curse of dimensionality for certified robustness via dual randomized smoothing. In *ICLR*, 2024. 1, 2

[48] Peng Xie, Yequan Bie, Jianda Mao, Yangqiu Song, Yang Wang, Hao Chen, and Kani Chen. Chain of attack: On the robustness of vision-language models against transfer-based adversarial attacks. In *CVPR*, 2025. 2

[49] Jiaming Zhang, Xingjun Ma, Xin Wang, Lingyu Qiu, Jiaqi Wang, Yu-Gang Jiang, and Jitao Sang. Adversarial prompt tuning for vision-language models. In *ECCV*, 2024.

[50] Jiaming Zhang, Junhong Ye, Xingjun Ma, Yige Li, Yunfan Yang, Yunhao Chen, Jitao Sang, and Dit-Yan Yeung. Anyattack: Towards large-scale self-supervised adversarial attacks on vision-language models. In *CVPR*, 2025.

[51] Yunqing Zhao, Tianyu Pang, Chao Du, Xiao Yang, Chongxuan Li, Ngai-Man Man Cheung, and Min Lin. On evaluating adversarial robustness of large vision-language models. *NeurIPS*, 2023. 1, 2, 6, 7, 8, 13

[52] Lianmin Zheng, Wei-Lin Chiang, Ying Sheng, Siyuan Zhuang, Zhanghao Wu, Yonghao Zhuang, Zi Lin, Zhuohan Li, Dacheng Li, Eric Xing, et al. Judging llm-as-a-judge with mt-bench and chatbot arena. *NeurIPS*, 2023. 7

Provable Robustness in Multimodal Large Language Models via Feature Space Smoothing

Supplementary Material

S.7. Proof of core theorem

S.7.1. Proof of lemma1

Note that:

$$\nabla \Phi^{-1}(\hat{S}_{x_c}(\mathbf{x})) = \frac{\nabla \hat{S}_{x_c}(\mathbf{x})}{\Phi'(\Phi^{-1}(\hat{S}_{x_c}(\mathbf{x})))}. \quad (\text{S.16})$$

Denote $p = \hat{S}_{x_c}(\mathbf{x})$, we can get that:

$$\Phi'(\Phi^{-1}(\hat{S}_{x_c}(\mathbf{x}))) = \frac{1}{\sqrt{2\pi}} \exp(-\frac{1}{2}(\Phi^{-1}(p))^2) \quad (\text{S.17})$$

Thus, we need to prove that for any unit direction u .

$$u \cdot \nabla \hat{S}_{x_c}(\mathbf{x}) \leq \frac{1}{\sqrt{2\pi}} \exp(-\frac{1}{2}(\Phi^{-1}(p))^2). \quad (\text{S.18})$$

For the left-hand side, we can get:

$$\nabla \hat{S}_{x_c}(\mathbf{x}) = \frac{1}{(2\pi)^{n/2}} \int_{\mathbb{R}^n} S_{x_c}(\mathbf{t}) (\mathbf{x} - \mathbf{t}) \exp(-\frac{1}{2}\|\mathbf{x} - \mathbf{t}\|^2) d\mathbf{t}, \quad (\text{S.19})$$

which can also be rewritten as follows:

$$\mathbb{E}_{X \sim \mathcal{N}(0, I)} [S_{x_c}(x + X) X \cdot u].$$

We can now claim that the supremum of the above quantity over all encoders $f : \mathbf{x} \rightarrow \mathbf{z}$, subject to the constraint that $p = \mathbb{E}[S_{x_c}(x + X)]$, is equal to:

$$\mathbb{E}[(X \cdot u) \mathbb{1}\{X \cdot u \geq -\Phi^{-1}(p)\}] = \frac{1}{\sqrt{2\pi}} \exp(-\frac{1}{2}(\Phi^{-1}(p))^2), \quad (\text{S.20})$$

which concludes the proof of Lemma 1.

S.7.2. Proof of Theorem1

From Lemma 1, we can get:

$$\|\mathbf{x} - \mathbf{x}'\| \geq \Phi^{-1}(\hat{S}_{\mathbf{x}}(\mathbf{x})) - \Phi^{-1}(\hat{S}_{\mathbf{x}}(\mathbf{x}')). \quad (\text{S.21})$$

As $\|\mathbf{x} - \mathbf{x}'\| \leq \epsilon$, we can get:

$$\Phi^{-1}(\hat{S}_{\mathbf{x}}(\mathbf{x}')) \geq \Phi^{-1}(\hat{S}_{\mathbf{x}}(\mathbf{x})) - \epsilon. \quad (\text{S.22})$$

Meanwhile, as $f_e(\mathbf{x})$ is a unit vector, using Equation 5 in the main paper, we can get that:

$$\begin{aligned} \hat{S}(\mathbf{x}) &= \frac{1}{2} \left(1 + \langle \mathbb{E}[f_e(\mathbf{x} + \varepsilon)], f_e(\mathbf{x}) \rangle \right) \\ &= \frac{1}{2} \left(1 + \langle \hat{f}_e(\mathbf{x}), f_e(\mathbf{x}) \rangle \right). \end{aligned} \quad (\text{S.23})$$

where $\langle \cdot, \cdot \rangle$ is the inner product. Hence, we can get:

$$\langle \hat{f}_e(\mathbf{x}), f_e(\mathbf{x}) \rangle = 2\hat{S}(\mathbf{x}) - 1. \quad (\text{S.24})$$

As $\|\hat{f}_e(\mathbf{x}')\| \leq 1$ and $\|f_e(\mathbf{x})\| = 1$, we can get:

$$\begin{aligned} \text{Cos}(\hat{f}(\mathbf{z}), f_e(\mathbf{x})) &= \frac{\langle \hat{f}(\mathbf{z}), f_e(\mathbf{x}) \rangle}{\|\hat{f}(\mathbf{z})\|} \\ &\geq \langle \hat{f}(\mathbf{z}), f_e(\mathbf{x}) \rangle \end{aligned} \quad (\text{S.25})$$

By the monotonicity of Φ ,

$$\hat{S}_{\mathbf{x}}(\mathbf{x}') \geq \Phi(\Phi^{-1}(\hat{S}(\mathbf{x})) - \epsilon). \quad (\text{S.26})$$

Combining Equations S.24, S.25, S.26, we thereby can derive that:

$$\text{Cos}(\hat{f}(\mathbf{x}'), f_e(\mathbf{x})) \geq 2\Phi(\Phi^{-1}(\hat{S}(\mathbf{x})) - \epsilon) - 1, \quad (\text{S.27})$$

which concludes the proof. For noise variance σ^2 , the same proof gives the bound with ϵ replaced by ϵ/σ .

S.8. Training details of PSM

S.8.1. Details of fine-tuning noise purifier

The Purifier \mathcal{P} is optimized in a self-supervised manner using the objective \mathcal{L}_p defined in Equation 9. We employ the ImageNet-pretrained 256×256 unconditional diffusion model² as the backbone of \mathcal{P} . All input images are resized to 256×256 .

To perform denoising, we instantiate a diffusion process consisting of 1,000 timesteps with a linear noise scheduler. Following common practices, the rescaled learned noise variance (i.e., "rescale_learned_sigma") is disabled to prevent instability during fine-tuning. We fine-tune the model for a total of 12,000 optimization steps using the AdamW optimizer, with an initial learning rate of 5×10^{-5} . An exponential moving average (EMA) with a decay rate of 0.99 is maintained throughout training to stabilize updates and improve the effective generalization of the learned purifier.

S.8.2. Details of training residual mapper

The structure of the proposed residual smoothness mapper \mathcal{M} is illustrated in Figure S.3. Each block is designed to refine the purified feature representation while preserving its

²<https://github.com/openai/guided-diffusion?tab=readme-ov-file>

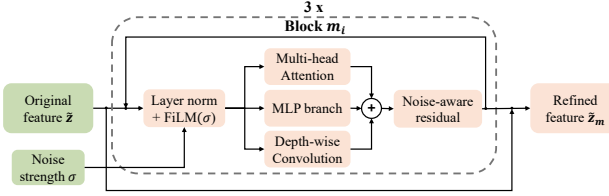


Figure S.3. Structure of the residual smoothness mapper.

statistical structure and ensuring that the refinement magnitude adapts smoothly to the injected noise magnitude σ . A single block consists of: (1) noise-aware LayerNorm-FiLM(σ) module, (2) multi-head attention, (3) a channel-wise MLP branch, (4) a depthwise convolution, and (5) a noise-aware residual module.

LayerNorm and FiLM(σ). Each block begins by normalizing the input feature and injecting noise-level conditioning:

$$\tilde{z}_i = \text{LN}(\tilde{z}_i), \quad [\gamma(\sigma), \beta(\sigma)] = \text{FiLM}(\sigma), \quad (\text{S.28})$$

where the FiLM module takes the scalar noise strength σ and outputs channel-wise affine parameters through a lightweight MLP:

$$\text{FiLM}(\sigma) = W_2 \phi(W_1 \sigma) \in \mathbb{R}^{2D}, \quad (\text{S.29})$$

with ϕ denoting a GELU activation. This modulation injects explicit noise awareness into each block: the transformation smoothly diminishes as $\sigma \rightarrow 0$, ensuring that the mapper leaves clean features nearly unchanged.

Main computation structure. Each $m_i(\cdot)$ contains three parallel refinement pathways:

- **Multi-head attention:** Applied only in the first block, the lightweight attention layer captures long-range structural dependencies, producing global-context features h_{attn} .
- **MLP branch:** A two-layer feed-forward network with GELU activation produces channel-wise refinement h_{mlp} .
- **Depthwise convolution:** A depthwise 1D convolution captures local continuity in the feature sequence and contributes h_{conv} .

The outputs are fused as:

$$h_i = h_{\text{attn}} + h_{\text{mlp}} + 0.5 h_{\text{conv}}, \quad (\text{S.30})$$

where the conv branch is down-weighted following design practices for local/global feature fusion.

Noise-aware residual. We first decompose h_i into a unit direction vector by $v_i = h_i / \|h_i\|$. To ensure that the refinement adapts smoothly to the noise level, we modulate its magnitude through two learnable functions of σ :

$$\begin{aligned} \alpha_i &= \text{softplus}(\text{MLP}_\alpha([\sigma, \log \sigma])), \\ \sigma^{\beta_i} &= \sigma^{\text{softplus}(\text{MLP}_\beta(\sigma))}. \end{aligned} \quad (\text{S.31})$$

Here, α_i controls the amplitude of the refinement, while β_i modulates the exponent of the noise term, enabling nonlinear noise–feature interactions. The residual update is then computed as

$$\Delta z_i = [(1 + \gamma(\sigma)) (v_i \cdot \alpha_i \sigma^{\beta_i}) + \beta(\sigma)] \odot \text{Scale}_i, \quad (\text{S.32})$$

where $\gamma(\sigma)$ and $\beta(\sigma)$ are FiLM-generated per-channel affine parameters, and Scale_i is a learnable per-channel damping factor initialized to 5×10^{-4} for stability. The next feature is then updated via

$$\tilde{z}_{i+1} = \tilde{z}_i + \Delta z_i. \quad (\text{S.33})$$

Overall effect of the mapper. The residual smoothness mapper thus provides the following benefits:

- **Noise-adaptive refinement:** FiLM(σ) and σ^β ensure the introduced modification decreases as $\sigma \rightarrow 0$, allowing the mapper to preserve the natural feature distribution while refining noisy features more aggressively.
- **Multi-scale feature enhancement:** Attention, MLP, and depth-wise convolution jointly capture global structure, per-channel adaptation, and local smoothness.
- **Stable and expressive residual learning:** Fixup-style initialization and Scale_i ensure training stability even with multiple stacked residual blocks.

Collectively, \mathcal{M} significantly enhances the smoothness and robustness of purified representations while avoiding distributional drift.

Training details. The mapper \mathcal{M} is trained in a self-supervised manner using the objective \mathcal{L}_m defined in Equation 13. We train \mathcal{M} for 8 epochs with a batch size of 16. The training process employs the AdamW optimizer with an initial learning rate of 2×10^{-4} and a cosine annealing learning rate schedule.

S.9. More experimental results

S.9.1. Implementation details for main results

Image captioning. For this task, we prompt the MLLM with “*Describe this image in one concise sentence, no longer than 20 words.*” to generate a caption for each input image. The predicted caption is then compared against the ground-truth caption and the adversarial target caption for evaluation.

Image classification. For this task, we prompt the MLLM with “*You are a precise visual classifier. What are the main objects in this image?: 0. rooster, 1. gibbon, 2. golden_retriever, 3. goldfish, 4. hen, 5. hognose_snake, 6. ice_bear, 7. killer_whale, 8. king_crab, 9. kite, 10. shark. Output only a single integer between 0 and 10 with no explanation, no text, no punctuation.*” to obtain the predicted class for each input image. All images in the dataset belong to classes 0–9, while class 10 (shark) is used as the adversarial target class. We then compute the ACC and ASR based

Table S.6. Experimental results on adversarial robustness of different defense methods and MLLMs on image classification tasks. **The Mapper \mathcal{M} is a lightweight U-Net.** The overall best results are shown in **bold**, and the best results without smoothing are underlined.

Model	Method	M-Attack [23]			FOA [14]			AttackVLM [51]		
		FCS↑	ACC↑	ASR↓	FCS↑	ACC↑	ASR↓	FCS↑	ACC↑	ASR↓
LLaVA-1.5-7B	Org.	0.427	8.2%	78.2%	0.437	3.8 %	81.0 %	0.458	6.0%	78.4%
	Smoothed org.	0.590	84.8%	0.2%	0.600	87.2%	0.2%	0.605	87.0%	0.2%
	FARE [37]	0.574	55.4%	14.6%	0.521	24.8%	39.8%	0.508	25.8%	45.0%
	Smoothed FARE	0.695	75.6%	5.2%	0.681	66.2%	1%	0.671	68.0%	1%
	TeCoA [29]	0.731	<u>67.4%</u>	<u>2%</u>	0.626	<u>29.0%</u>	<u>20.0%</u>	0.592	<u>33.6%</u>	<u>17.8%</u>
	Smoothed TeCoA	0.790	70.6%	0.6%	0.714	58.8%	0.8%	0.712	56.4%	0.4%
CLIP-L14	Org.	0.427	18.0%	37.2%	0.437	10.0 %	52.4 %	0.458	16.0%	48.4%
	Smoothed org.	0.590	88.0%	0.4%	0.600	90.0%	0.4%	0.604	90.4%	0.4%
	FARE [37]	0.574	70.4%	5.2%	0.521	<u>42.0%</u>	<u>14.4%</u>	0.508	35.6%	24.4%
	Smoothed FARE	0.695	84.4%	0%	0.682	78.4%	0%	0.671	76.4%	0%
	TeCoA [29]	0.731	<u>81.2%</u>	<u>2.4%</u>	0.626	39.2%	20.2%	0.592	<u>35.8%</u>	<u>24.4%</u>
	Smoothed TeCoA	0.790	87.6%	1.2%	0.714	75.6%	2.4%	0.712	73.2%	2.0%

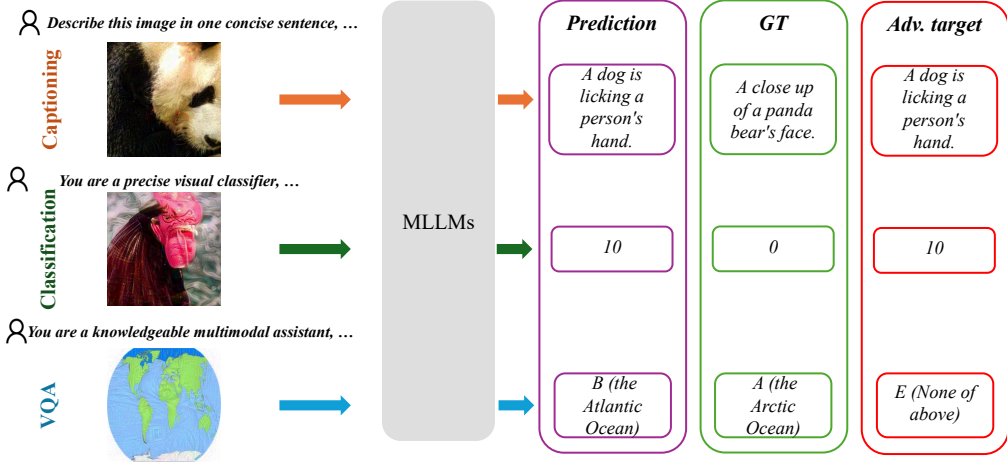


Figure S.4. Illustration of the evaluation process.

on the predicted labels, the ground-truth labels, and the adversarial target label.

VQA. For this task, we prompt the MLLM using the provided question associated with each input image and ask it to predict the corresponding answer. An example prompt is as follows: *"You are a knowledgeable multimodal assistant. Please answer the multiple-choice question ONLY by outputting the single letter of the correct option. Do not include explanations or extra text. Question: Which ocean is highlighted? Options: A. the Arctic Ocean B. the Atlantic Ocean C. the Pacific Ocean D. the Southern Ocean E. None of the above. If the visual information is not clear or uncorrelated with the questions, you should select the choice: None of the above. Answer with exactly one letter from the options above (e.g., A)."* In this evaluation, each question has a unique correct answer among the listed options, except for "None of the above," which is reserved for the ad-

versarial target. The adversarial objective is to induce the MLLM to incorrectly choose "None of the above".

An illustration of the implementation process is shown in Figure S.4.

S.9.2. Experimental results of using a lightweight U-net as noise purifier

The comparative results of different defense methods for image classification are summarized in Table S.6. In this experiment, **the original diffusion-based noise purifier is replaced with a lightweight U-Net denoiser containing approximately 43.7M parameters.** The results show that with this compact denoiser, FS-PSM consistently achieves strong and superior robustness, outperforming adversarial training-based baselines by a substantial margin. Furthermore, integrating FS-PSM with existing defenses yields additional robustness gains, leading to consistently favorable

Table S.7. Experimental results on adversarial robustness of different defense methods and MLLMs on image classification tasks. The attack bound $\epsilon = 32/255$.

Model	Method	FOA [14]		
		FCS \uparrow	ACC \uparrow	ASR \downarrow
LLaVA-1.5-7B	Org.	0.37	3.6%	78.6%
	Smoothed org.	0.512	35.2%	24.2%
	FARE [37]	0.408	10.4%	64.2%
	Smoothed FARE	0.605	48.4%	19.2%
	TeCoA [29]	0.454	12.0%	29.6%
	Smoothed TeCoA	0.576	32.0%	9.6%

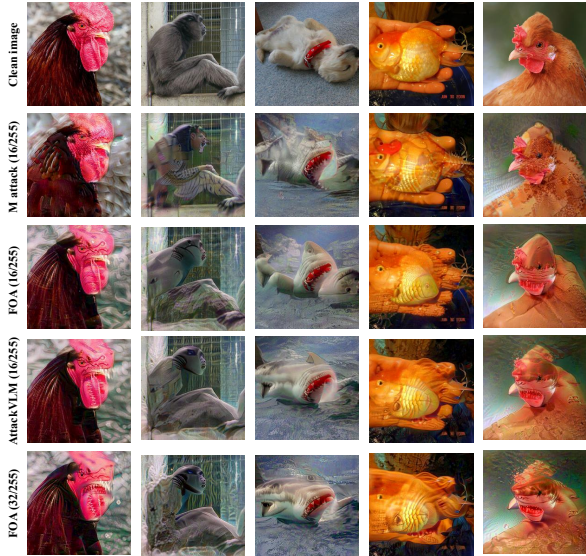


Figure S.5. Visualization of the adversarial examples.

improvements across all evaluated settings. These results collectively demonstrate the effectiveness and generalizability of the proposed method.

S.9.3. Experimental results on large attack bound

The experimental results under a large adversarial perturbation of $\epsilon = 32/255$ are presented in Table S.7. In addition, Figure S.5 provides visualizations of the adversarial examples generated by different attacks and perturbation bounds. These results show that nearly all existing defenses show great performance drop under such a strong attack. Under this challenging setting, the best accuracy is obtained by integrating FS-PSM with FARE, reaching 48.4% on LLaVA, while the lowest ASR (9.6%) is achieved by combining FS-PSM with TeCoA. These findings further highlight the effectiveness and adaptability of the proposed framework, even against large-magnitude adversarial perturbations.

Table S.8. Analysis of the robustness-efficiency trade-off of using different n_0 .

Model	n_0	Robustness			Efficiency
		FCS \uparrow	ACC \uparrow	ASR \downarrow	
LLaVA-1.5-7B (diffusion purifier)	1	0.595	86.2%	0.6%	0.28
	2	0.652	88.4%	0.4%	0.41
	4	0.697	88.8%	0.4%	0.66
	8	0.719	89.6%	0.4%	1.12
	16	0.728	89.2%	0.4%	2.10
	1	0.494	84.4%	0.2%	0.20
LLaVA-1.5-7B (lightweight purifier)	2	0.565	85.4%	0%	0.24
	4	0.600	87.2%	0.2%	0.32
	8	0.623	87.8%	0.4%	0.49
	16	0.643	86.8%	0.4%	0.84

S.9.4. Analysis of robustness-efficiency trade-off

The robustness–efficiency trade-off results are summarized in Table S.8. In this experiment, we adopt the strong FOA attack as the adversary and report the average inference time per sample on LLaVA-1.5-7B using a single RTX 4090 GPU. The results show that increasing the sampling number n_0 consistently improves the FCS under adversarial perturbations. Specifically, increasing n_0 from 0 to 16 raises FCS from approximately 0.595 to 0.728, which aligns with our theoretical analysis in Section 3. However, this robustness gain comes at a substantial computational cost. For example, increasing n_0 from 4 to 16 raises the inference latency from 0.66 seconds to 2.10 seconds per sample, revealing an inherent trade-off between robustness and efficiency.